Auton Robot (2007) 23: 147–159
DOI 10.1007/s10514-007-9037-8

Numerical comparison of steering geometries for robotic vehicles by modeling positioning error

Joaquín Gutiérrez · Dimitrios Apostolopoulos · José Luis Gordillo

Received: 8 September 2006 / Revised: 3 April 2007 / Accepted: 4 April 2007 / Published online: 23 May 2007

Abstract This paper describes an analytical method for modeling the positioning error of a robotic vehicle and examines how the metric of this error can be used to compare the geometries of various steering configuration. Positioning error can be caused by many factors stemming from the robot's hardware and software configurations and the interaction between the robot and its environment. A slip motion model that captures the effects of key factors that contribute to positioning error is presented. Robot kinematic models with and without slippage are reformulated and used to perform an in-depth assessment and characterization of positioning error. The method is applied to three characteristic advance and steering configurations: Ackermann, articulated, and explicitly steered. This analysis serves as a quantitative evaluation of the properties of the steering geometries for path tracking under identical slippage conditions. The method can also be used as a tool for comparing robot configurations to make trade-off decisions early in the design process, as it allows for derivation of predicted performance values of alternative steering geometries.

Keywords Positioning error · Simulation · Autonomous vehicles

J. Gutiérrez (✉)
CIBNOR, La Paz, BCS, Mexico
e-mail: joaquing04@cibnor.mx

D. Apostolopoulos
The Robotics Institute CMU, Pittsburgh, PA, USA
e-mail: da1v@cs.cmu.edu

J.L. Gordillo
Tecnológico de Monterrey, Monterrey, NL, Mexico
e-mail: JLGordillo@itesm.mx

1 Introduction

Wheeled robotic vehicles perform tasks in hazardous or remote environments and can move toward a desired site to execute specialized tasks (such as exploration and environmental monitoring) in situations where stationary robots are limited. Several implementations of robotic vehicles have used light trucks or buses (Thorpe 1997; Redmill and Ozguner 1999), and land vehicles from agriculture (Stombaugh 1998; Pilarski et al. 2002), construction (Stentz et al. 1999; Cannon 1999; Gambao and Balaguer 2002), utility (Trebi-Ollennu and Dolan 1999; Coombs et al. 2000; Fong et al. 2003) and mining applications (Stentz 2001; Thrun et al. 2003; Gutierrez et al. 2004). The development of original designs for planetary exploration has also demonstrated the potential of wheeled robotic vehicles (Rollins et al. 1998; Fiorini 2000; Tunstel et al. 2002; Muirhead 2004). These diverse, demanding applications produce a variety of robotic configurations that depend on vehicle kinematics; in particular, the advance and steering geometry, which is the physical interface between the robotic vehicle and its environment. Although the derivation and classification of wheeled vehicle kinematics and their controllability models have been investigated (Muir and Neuman 1987; Alexander and Maddocks 1989; Laumond 1993; Samson 1995; Campion et al. 1996), the current state-of-practice rarely involves explicit reasons for using them and instead employs precedent robotic and conventional vehicles (Dudzinski 1989; Colyer and Economou 1998; Altafini 1999b). With the exception of the Nomad vehicle, which used analytical procedures and mobility metrics for the design and testing of its locomotion system (Apostolopoulos 2001), there are few descriptions of the analysis process for choosing the advance and steering geometry during the configuration and implementation of such robotic systems. Furthermore, this sub-

ject and its relationship with other robotic components (such as power, computational demand and sensor placement) are usually deferred until after physical prototyping. They are treated as topics of engineering and *ad hoc* processes, consisting of rough estimates of performance requirements.

This paper examines steering kinematics as a criterion that should be taken into account during the configuration and automation process. It compares three widely known steering geometries: Ackermann Steering (AS), aRticulated Steering (RS), and Explicit independent Steering (ES), to select the adequate steering kinematics that improves the robotic vehicle's function.

A general method is presented to numerically analyze these steering geometries by considering differences in positioning error. Although the skid vehicles are used broadly in robotics applications, these vehicles are beyond this analysis; because steering motions are controlled by using the difference in the wheel velocities to turn rather than turning on a steering axle. Section 2 presents the relevant works related to positioning error. Sections 3 and 4 introduce the complete derivation of the reformulated kinematic models and positioning error equations. Section 5 presents the simulation performance of every steering scheme under certain conditions, applied experimental data from trials into an underground mining environment. In Sect. 6 the three steering models are compared using a positioning error ratio metric. Finally, the conclusions are presented in Sect. 7.

2 Related work

Research work in numerous techniques for estimating position has been conducted to enhance vehicle performance, reporting numerous techniques (Everett 1995; Borenstein et al. 1997). Some techniques that are based on external sensors, such as GPS, are excluded from specific environments, such as underground mining or planetary exploration (Barshan and Durrant-Whyte 1995; Dissanayake et al. 2001). Other schemes require complete knowledge of or additional structure in the environment. An essential method for estimate vehicle position is dead reckoning, which is used mainly in hostile and unknown environments. This method is based on the use of simple kinematic models that integrate incremental motion information from internal sensors (such as wheel and steer encoders or inertial sensors) to provide low-level control and estimate vehicle position.

Dead reckoning suffers from positioning error due to accumulation of sensor errors (Chung et al. 2001; Kelly 2004). Furthermore, this method is affected by many unpredictable factors that are extremely difficult to model accurately and involve a combination of vehicle parameters (e.g. advance and steering mechanism), environment conditions (e.g. terrain properties), and vehicle-environment interaction. A solution is to select an advance and steering system that is less prone to positioning error in the expected environment. Because this system is the physical interface between the environment and the robotic vehicle, it is necessary to systematically analyze and identify the kinematic requirements of the steering geometry that improve position estimation. In our analysis of steering kinematics, a slip motion model is chosen to represent the combination and impact of these factors. Hence the error in vehicle positioning is estimated for the case of kinematic model with explicit slip against an ideal model without slip. The steering mechanisms are then quantitatively compared to select the vehicle kinematics that minimizes the error in position estimation.

3 Kinematic models

Kinematic models for the four-wheeled vehicles (AS, RS, and ES) are reformulated from general geometry that include ideal and slip behavior for the steering schemes. The definition of these models are based on the derivation of Altafini (1999a) and the slippage representation of Shiller and Sundar (1998), to include the perturbed factors in the vehicle position as two slip variables. The rear and front slip angles, α and β, are the angles between the linear velocity of the vehicle and the rear and front axes, respectively.

The geometries of the vehicles are simplified by collapsing both front and rear wheels into a single wheel at the midpoint of every axle, known as the bicycle model (Latombe 1991). The rear position of the vehicle relative to some fixed coordinate system is denoted by x_r and y_r. The angle θ denotes the vehicle orientation with respect to the x axis. The length of vehicle is L, considering the distance between front and rear axles. The linear velocity of the vehicle is V; the steering angle is γ.

The analysis considers a steady-state turning radius R at the instantaneous center of curvature (ICC), where γ is a constant (i.e. $\dot{\gamma} = 0$) to compute the position error for every steering vehicle.

3.1 Ackermann steering model

The AS geometry consists of rear wheels that are driven with fixed orientation and front wheels that are steered (Fig. 1).

• AS model with slip. In this analysis, the constraint of zero velocity in the direction of the axles (nonholonomic constraint) is considered as the slip motion, and the rigid body constraint. Thus, the kinematic model that introduces the slip factor to estimate the position of the vehicle is formulated to obtain:

$$\begin{bmatrix} \dot{x}_{AS_S} \\ \dot{y}_{AS_S} \\ \dot{\theta}_{AS_S} \end{bmatrix} = \begin{bmatrix} V\cos(\theta-\alpha) \\ V\sin(\theta-\alpha) \\ \frac{V\sin(\gamma+\alpha-\beta)}{L\cos(\beta-\gamma)} \end{bmatrix}. \quad (1)$$

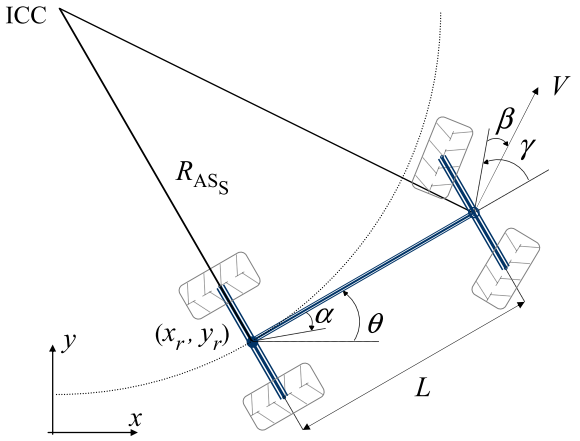

Fig. 1 AS kinematic geometry: including slip angles that impact the ideal radius (R_{AS}), and produce an slip radius R_{AS_S} due to slip motion leads to an error in position estimation

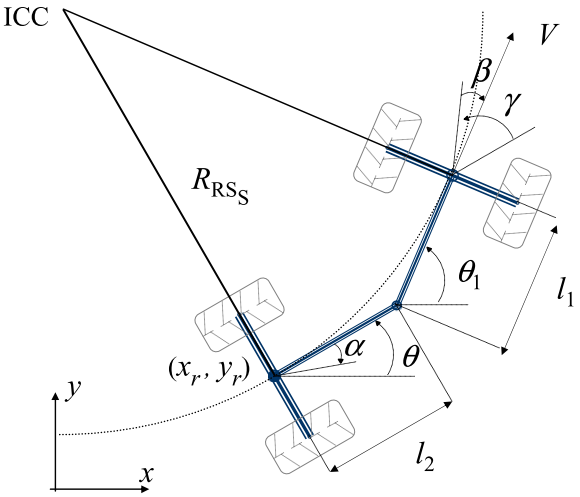

Fig. 2 RS kinematic geometry: including slip angles that produce the slip radius R_{RS_S} instead of the ideal radius R_{RS}

• AS model without slip. The kinematic model of the vehicle is derived from (1), excluding the slipping condition between the wheels and the ground (i.e. $\alpha = 0$ and $\beta = 0$). It is given as:

$$\begin{bmatrix} \dot{x}_{AS} \\ \dot{y}_{AS} \\ \dot{\theta}_{AS} \end{bmatrix} = \begin{bmatrix} V\cos(\theta) \\ V\sin(\theta) \\ \frac{V\sin(\gamma)}{L\cos(\gamma)} \end{bmatrix}. \tag{2}$$

3.2 Articulated steering model

An articulated vehicle is composed of two bodies connected by a kingpin hitch, a front and a rear body that can rotate relative to one other (Fig. 2). Each body has a single axle with two fixed wheels (non-steerable). The steering behavior is achieved by driving the articulation joint located between the front and rear axles.

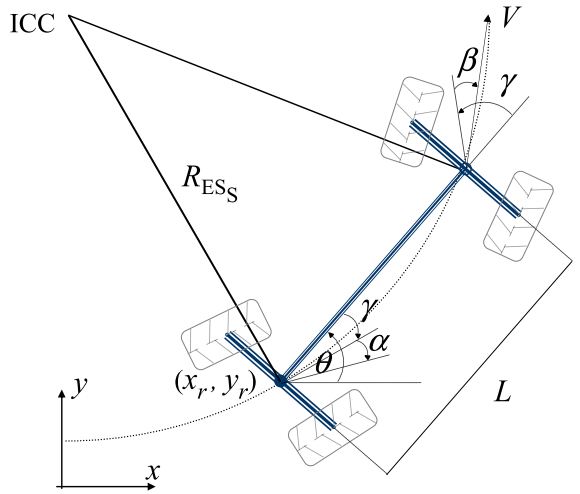

Fig. 3 ES kinematic geometry becomes a bi-steerable (double Ackermann steering), assuming a steady-state turning

The lengths of the front and rear bodies are denoted by l_1 and l_2, respectively. The length of the entire vehicle is $L = l_1 + l_2$. The angles θ and θ_1 denote the orientation of the vehicle bodies with respect to the x axis. The steering angle γ is given by $\gamma = \theta_1 - \theta$.

• RS model with slip. The kinematic model of the vehicle formulated with the presence of the slip factor is given by:

$$\begin{bmatrix} \dot{x}_{RS_S} \\ \dot{y}_{RS_S} \\ \dot{\theta}_{RS_S} \end{bmatrix} = \begin{bmatrix} V\cos(\theta-\alpha) \\ V\sin(\theta-\alpha) \\ \frac{V\sin(\gamma+\alpha-\beta)-l_1\dot{\gamma}\cos(\beta)}{l_1\cos(\beta)+l_2\cos(\beta-\gamma)} \end{bmatrix}. \tag{3}$$

• RS model without slip. The kinematic model of the vehicle derived from (3) under the constraints of rigid body and rolling without slipping is given by:

$$\begin{bmatrix} \dot{x}_{RS} \\ \dot{y}_{RS} \\ \dot{\theta}_{RS} \end{bmatrix} = \begin{bmatrix} V\cos(\theta) \\ V\sin(\theta) \\ \frac{V\sin(\gamma)-l_1\dot{\gamma}}{l_1+l_2\cos(\gamma)} \end{bmatrix}. \tag{4}$$

3.3 Explicit steering model

The ES vehicle structure is designed so that all four wheels can be driven and steered individually. However, under the assumption of steady-state turning, the ES model becomes a bi-steerable vehicle as depicted in Fig. 3 as a double Ackermann steering. This bi-steerable behavior has a linear relationship between the front steering angle and rear steering angle. The front steering angle γ is equal to the rear steering angle γ in the opposite direction.

• ES model with slip. The kinematic model of the vehicle with the slip constraint is given by:

$$\begin{bmatrix} \dot{x}_{ES_S} \\ \dot{y}_{ES_S} \\ \dot{\theta}_{ES_S} \end{bmatrix} = \begin{bmatrix} V\cos(\theta-\gamma-\alpha) \\ V\sin(\theta-\gamma-\alpha) \\ \frac{V\sin(2\gamma+\alpha-\beta)}{L\cos(\beta-\gamma)} \end{bmatrix}. \tag{5}$$

• ES model without slip. The kinematic model of the vehicle reformulated from (5), assuming rolling without slipping and rigid body constraint, is:

$$\begin{bmatrix} \dot{x}_{ES} \\ \dot{y}_{ES} \\ \dot{\theta}_{ES} \end{bmatrix} = \begin{bmatrix} V\cos(\theta-\gamma) \\ V\sin(\theta-\gamma) \\ \frac{V\sin(2\gamma)}{L\cos(\gamma)} \end{bmatrix}. \tag{6}$$

The kinematic models described by (1–6) are similar to the models in (Muir and Neuman 1987; Alexander and Maddocks 1989; Dudzinski 1989; Laumond 1993; Samson 1995; Campion et al. 1996; Scheding et al. 1997; Large et al. 2000), which lead to the derivation and classification of kinematic, dynamic, and controllability models.

4 Positioning error

From the kinematic models with slip perturbation, it can be observed that the vehicle motion depends not only on control inputs V and γ and vehicle length L, but also on the slip angles. The vehicle heading is given by the slip angle α and orientation angle θ. The change rate of orientation $\dot{\theta}$ is a function of the steering angle γ and both slip angles α and β. Furthermore, based on the assumption that the vehicle develops a steady-state motion turning (i.e. $\dot{\gamma}=0$), the rate of orientation change is given by $\dot{\theta}=V/R$, depending on turning radius R. Thus, any change experienced in the radius due to slip leads to an error in position estimation.

This effect of the slip angles on vehicle motion is expressed as a normalized Positioning Error Ratio (PER), which is the ratio of the slip radius against the ideal radius. In this context, the PER for the AS, RS, and ES geometries are formulated as follows:

• Ackermann PER

Referring to the geometry of the AS vehicle (Fig. 1) and (2), the radius without slip depends on the vehicle length L and γ:

$$R_{AS} = \frac{L\cos\gamma}{\sin\gamma}.$$

Solving for slip radius of AS vehicle from (1):

$$R_{AS_S} = \frac{L\cos(\beta-\gamma)}{\sin(\gamma+\alpha-\beta)}.$$

Thus, the ratio for Ackermann steering (PER_{AS}) is denoted by:

$$PER_{AS} = 1 - \frac{\cos(\beta-\gamma)\sin\gamma}{\cos\gamma\sin(\gamma+\alpha-\beta)}.$$

• Articulated PER

Referring to the RS geometry (Fig. 2) and (3) and (4), the ratio for Articulated steering (PER_{RS}) is formulated as:

$$PER_{RS} = 1 - \frac{[l_1\cos\beta + l_2\cos(\beta-\gamma)]\sin\gamma}{(l_1+l_2\cos\gamma)\sin(\gamma+\alpha-\beta)}.$$

• Explicit PER

Referring to the ES geometry (Fig. 3), the ratio for Explicit vehicle (PER_{ES}) from (5) and (6) becomes:

$$PER_{ES} = 1 - \frac{\cos(\beta-\gamma)\sin 2\gamma}{\cos\gamma\sin(2\gamma+\alpha-\beta)}.$$

As was mentioned earlier, the key issue addressed in this paper is to compare three steering geometries to minimize the error in position estimation. This error is caused by many factors that are unpredictable and extremely difficult to model accurately. Slip motion was chosen to represent the combination and effect of these factors, since the slip angles are uncertain parameters that depend on vehicle speed, steering angle and terrain properties. In this analysis, we assume that the slip angles are a percentage of the steering angle γ (i.e. $k_\alpha=\alpha/\gamma$ and $k_\beta=\beta/\gamma$). The expected radius is dependent on the steering angle, a physical input of the system. Thus, considering these percentages and by introducing the length ratio ($r=l_1/l_2$) for RS vehicle, the PER equations result in:

$$PER_{AS} = 1 - \frac{\cos(\gamma[k_\beta-1])\sin\gamma}{\cos\gamma\sin(\gamma[1+k_\alpha-k_\beta])}, \tag{7}$$

$$PER_{RS} = 1 - \frac{[r\cos(k_\beta\gamma)+\cos(\gamma[k_\beta-1])]\sin\gamma}{[r+\cos\gamma]\sin(\gamma[1+k_\alpha-k_\beta])}, \tag{8}$$

$$PER_{ES} = 1 - \frac{\cos(\gamma[k_\beta-1])\sin 2\gamma}{\cos\gamma\sin(\gamma[2+k_\alpha-k_\beta])}. \tag{9}$$

To compute the ratio of each steering mechanism, we assume particular values of the slip angles between 0% and 70% of steering angle. This covers several possible sceneries and reported data in the literature (Gillespie 1992; Dixon 1996; Shiller and Sundar 1998). For example, Scheding et al. (1999) reports estimated values for the slip angles in experimental trails developed in underground mining using an articulated Load, Haul and Dump truck (LHD). The values were estimated from real data using a statistical filter. The percentage for slip angle α is estimated as 66.19% with respect to steering angle γ, whereas that it is 16.62% for slip angle β. These estimated values are applied to PER equations under the disposition shown in Table 1, as the experimental data to investigate the impact on the steering schemes.

Table 1 Percentages of the slip angles: k_α and k_β

Case	I		II		III	
	k_α	k_β	k_α	k_β	k_α	k_β
(a)	00	00	00	00	00	00
(b)	00	10	10	10	10	00
(c)	00	30	30	30	30	00
(d)	00	50	50	50	50	00
(e)	00	70	70	70	70	00

5 Positioning error simulation

5.1 PER analysis

In this simulation, the steering mechanisms perform various curve radii at different vehicle lengths. The steering angle γ required is fixed along the turning radius at constant forward velocity to maintain the vehicle under steady-state conditions. The position error ratios simulated to the radii and vehicle length inputs are used for comparing the response to the slippage of the three steering schemes. The normalized results for AS, RS, and ES vehicles are shown in Figs. 4, 5, and 6, respectively. Referring to these results, several observations are made:

- The slip angle β produces a bigger error than the slip angle α under similar estimations in the three steering mechanisms. This can be observed in the plotted ratios (**I**) compared with the ratios produced by case (**III**), for all percentage combinations from (**a**) to (**e**).
- A combination of both slip angles produce smaller ratio than the ratio produced by the biggest slip angle of this combination. For instance, case (**II**) is smaller than plotted cases (**I**) and (**III**). When the slip angles are equal, this effect is minor. Both slip angles trend to cancel their effect on the performed radius of the case (**II**), that is clear in the term $(\gamma + \alpha - \beta)$ from (1), (3), and (5); besides, the effect is minor at lower percentages.
- If $\alpha > \beta$, case (**III**), the ratio has the tendency to increase while the radius is increased and the vehicle length (wheelbase) is reduced, a behavior inversely proportional to the relation L/R. In the rest of cases where $\alpha \leq \beta$, cases (**I**) and (**II**), there is a proportional behavior to relation L/R.

Furthermore, when the radius increases the ratio L/R is quite small, and the steering angle γ is small and the length of the vehicle can be negligible. To compute the error ratio, assume that $\sin\gamma = \gamma$ and $\cos\gamma = 1$ when the steering angle is expressed in radians. The ratio equation of an AS vehicle can be simplified as:

$$PER_{AS_{\gamma\approx 0}} = 1 - \frac{1}{[1 + k_\alpha - k_\beta]}.$$

The ratio equation of an RS vehicle for a small steering angle γ is given as:

$$PER_{RS_{\gamma\approx 0}} = 1 - \frac{1}{[1 + k_\alpha - k_\beta]}.$$

The ratio equation of an ES vehicle for a small steering angle γ is given as:

$$PER_{ES_{\gamma\approx 0}} = 1 - \frac{2}{[2 + k_\alpha - k_\beta]}.$$

Thus, if $R \gg L$ the positioning error ratio is only a function of the slip angles α and β.

5.2 PER accumulation

Even small positioning errors have an impact on vehicle position estimation that accumulates with the time. This can be seen from kinematic models that provide an estimate of the position and orientation or heading of the vehicle with respect to some coordinate system. The deviation from the ideal performance of the radius has a significant impact on the computation of the vehicle heading (θ), propagating errors in vehicle position (x and y).

Figure 7 shows the estimated position of the vehicle, considering a certain percentage of the slip angles while the vehicles perform a complete turn. In particular, assume that the vehicles perform a steady turn of radius R (3 m) that is centered at the origin of the coordinates. The circular trajectory is traced counterclockwise at a constant velocity ($V = 1$ m/s) starting with the rear axle midpoint of each vehicle located at point $(0, -3)$. The length of the vehicle is 2 m.

The vehicle position is estimated using the discrete kinematic models. They are derived from the previous kinematic models that include slip angles that are parameterized by a random process consisting of a sequence of discrete values of fixed length (Random walk or Brownian motion), which depend on steering angles $\gamma_{AS} = 33.69$, $\gamma_{RS} = 36.87$, and $\gamma_{ES} = 19.47$, respectively (Fig. 8). In Fig. 7, both under-steering and over-steering occurred due to the magnitudes of the slip angles. All of the vehicles experienced an over-steering estimation that is related to a bigger rear slip angle α than front slip angle β until step 150. An under-steering occurred due to a bigger front slip angle β from step 200 in the Fig. 8. In this simulation, the ES vehicle is closer to the circular trajectory end. Fig. 9 shows the accumulated error, which is calculated as the distance between two points in the plane: the ideal position and the position that the vehicle experienced due to slip angles.

The accumulated error in position estimation for the ES vehicle is smaller than the error of the AS and RS vehicles by more than 50%. The AS error and RS error are similar. This shows that the results of the analysis of the vehicle

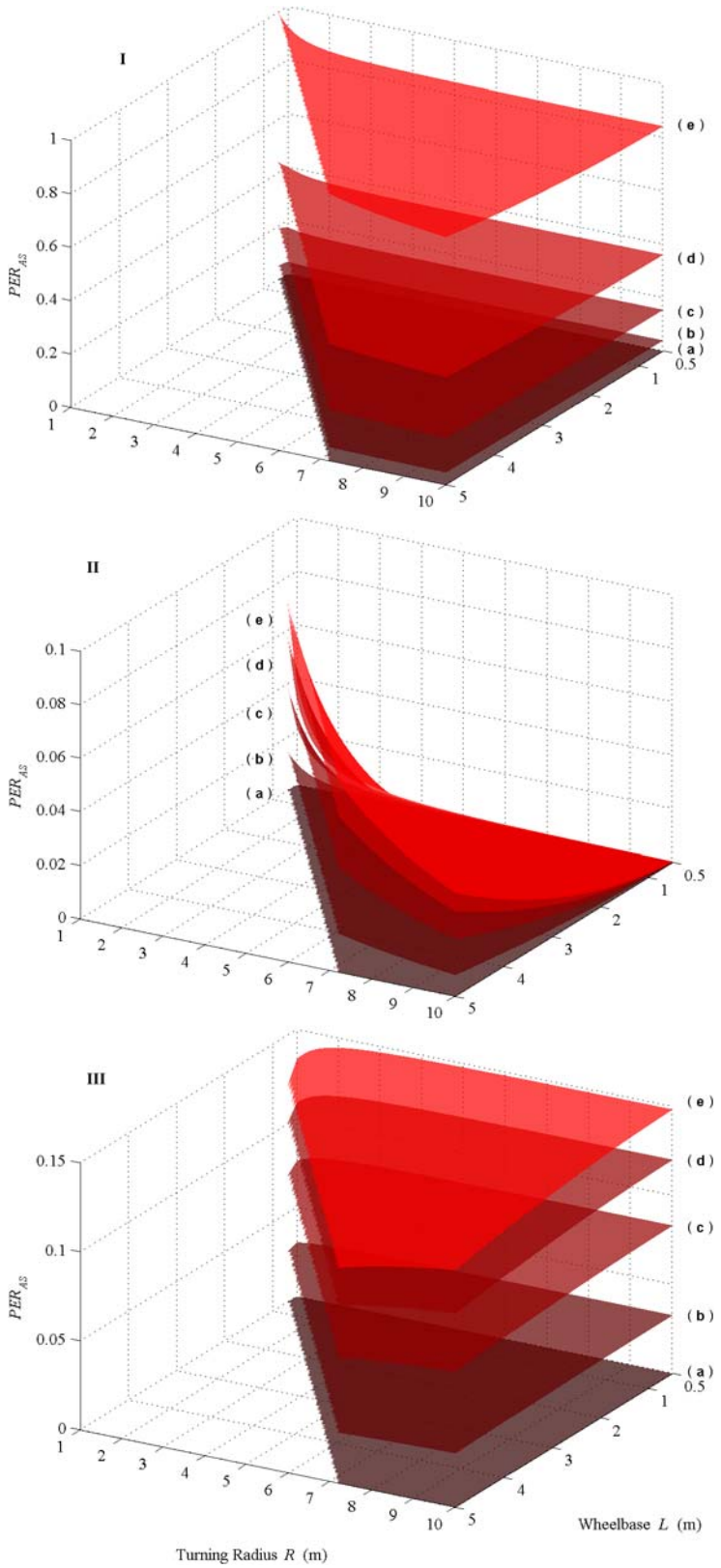

Fig. 4 Positioning error ratio for Ackermann steering: (**I**) $\alpha = 0$, (**II**) $\alpha = \beta$, and (**III**) $\beta = 0$, using the different proportion for k_α and k_β of Table 1

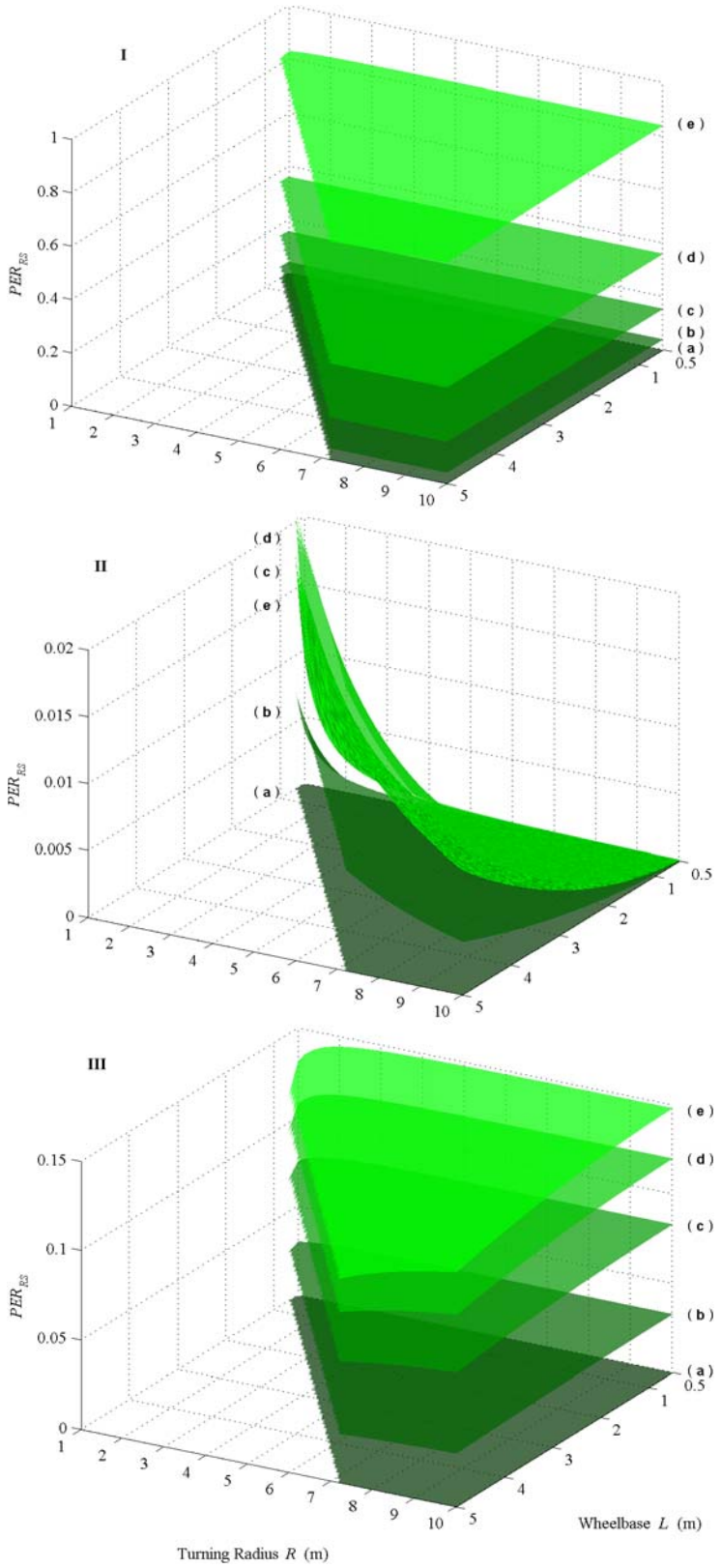

Fig. 5 Positioning error ratio for Articulated steering: (**I**) $\alpha = 0$, (**II**) $\alpha = \beta$, and (**III**) $\beta = 0$, using the different proportion for k_α and k_β of Table 1

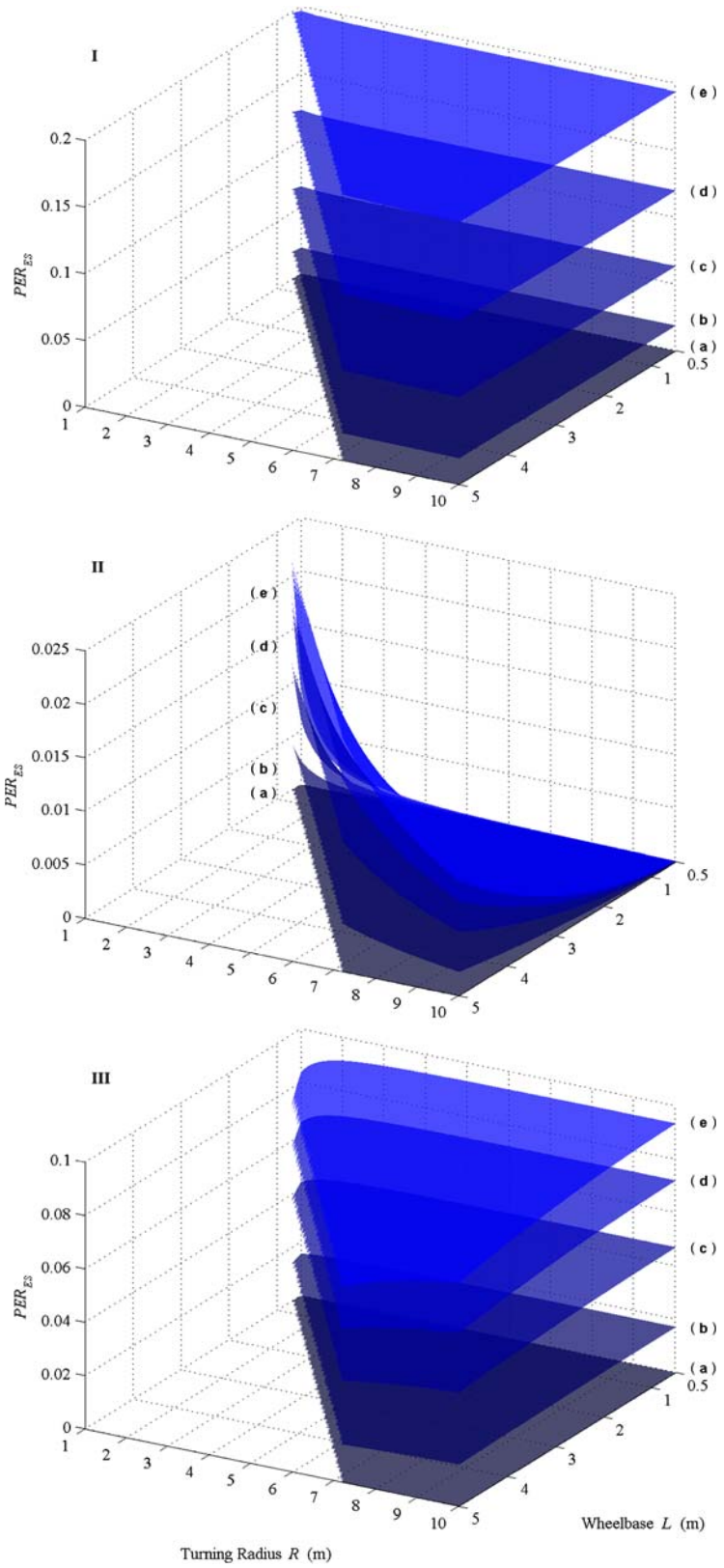

Fig. 6 Positioning error ratio for Explicit steering: (**I**) $\alpha = 0$, (**II**) $\alpha = \beta$, and (**III**) $\beta = 0$, using the different proportion for k_α and k_β of Table 1

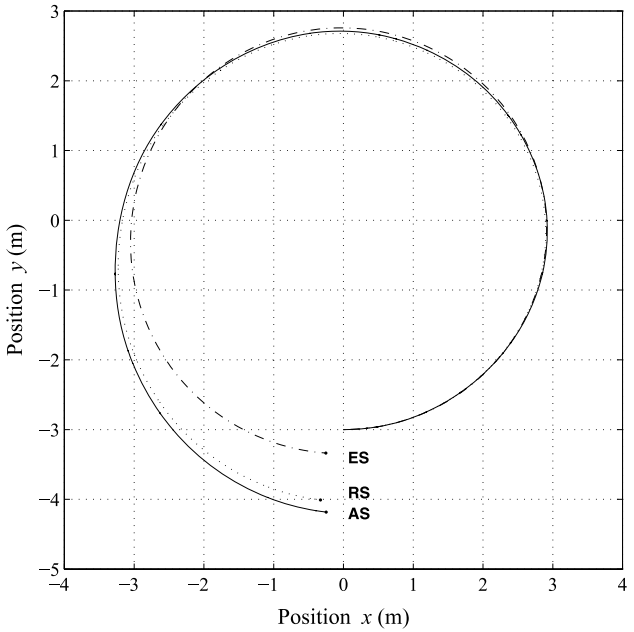

Fig. 7 Accumulated PER of Ackermann, Articulated and Explicit vehicles while performing a steady turn ($R = 3$ m)

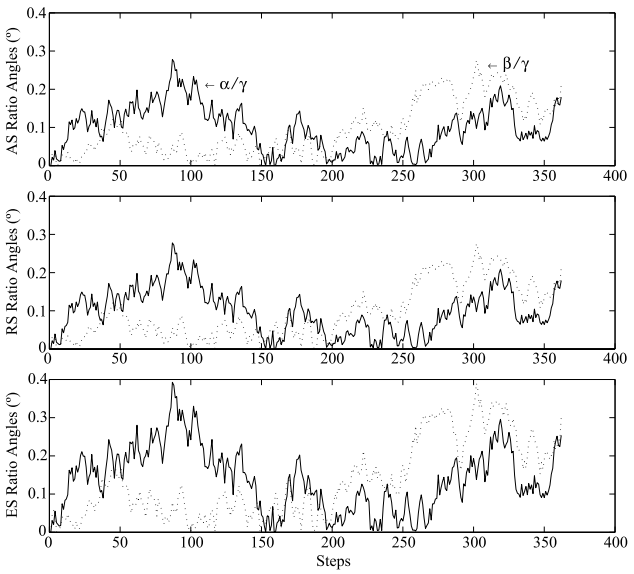

Fig. 8 Random estimation of the slip angles: 360 random values for slip angles α and β with respect to the steering angle γ, respectively

positioning should be taken into account when choosing a robotic vehicle configuration.

6 Discussion and comparison

Positioning error has been estimated for Ackermann, Articulated, and Explicitly steered vehicles. This error is calculated as the ratio between an ideal and a slip turning radius,

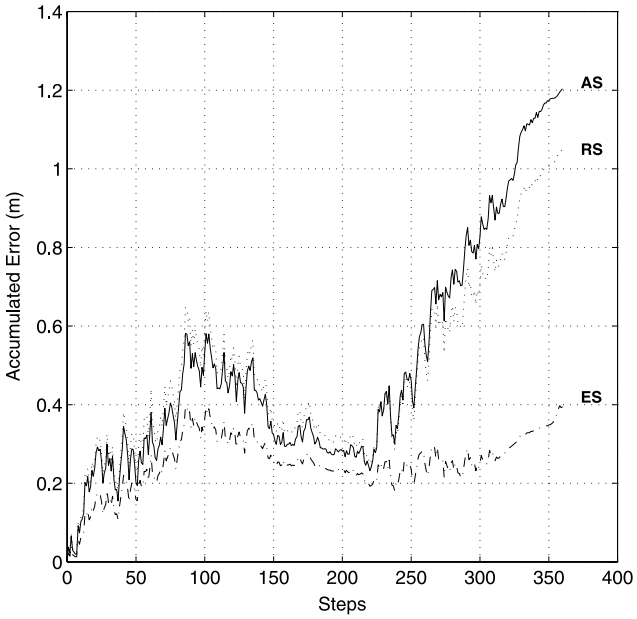

Fig. 9 Accumulated error of Ackermann, Articulated and Explicit vehicles while performing a steady turn. The error is calculated as the distance between the ideal position and the position that the vehicle experienced due to slip angles

in the context of the same conditions. The results address the following comparisons:

1. The results show an advantage for the ES vehicles in minimizing error in vehicle positioning. The ES ratio was more than 60% more accurate than the AS and RS ratios (as seen in Fig. 10). Therefore, it can be expected to have a better accuracy for vehicle position estimation through dead-reckoning.
2. The AS and RS vehicles present similar ratios. An AS vehicle had an error ratio that was 10% better than an RS vehicle at a small turning radius for case (**III**). However, this behavior is the opposite for cases (**I** and **II**). Therefore, it can be expected that AS and RS vehicle will have comparable accuracy for vehicle position estimation. This improvement tends to be negligible at a large turning radius, where AS and RS vehicles produce similar ratios.
3. All three steering mechanisms have a tendency to minimize the ratio when the wheelbase is increased, although this advance is negligible when the turning radius is increased. Therefore, the expected improvement is proportional to the relationship L/R.

Note that the ES vehicle requires a minor steering angle γ to perform a specific turning radius in comparison with AS and RS vehicles. However, this behavior is also maintained when these vehicles perform a specific steering angle γ, as shown in Fig. 11. Furthermore, the ES vehicle continues to show an enhanced position estimation and accumulated error under the same magnitude of slip angle percentage to

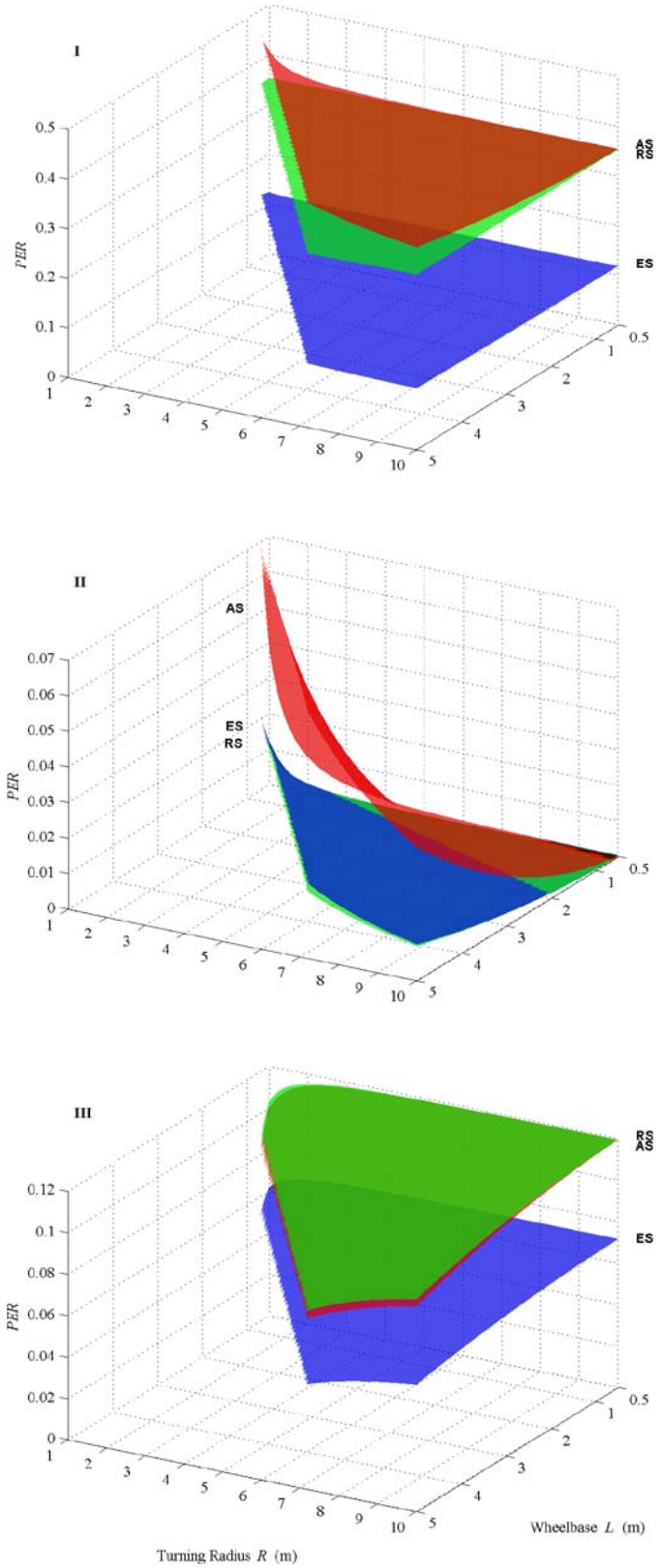

Fig. 10 PER comparison of Ackermann, Articulated and Explicit steering: (**I**) $k_\alpha = 16.62\%$ and $k_\beta = 66.19\%$, (**II**) $k_\alpha = 66.19\%$ and $k_\beta = 66.19\%$, and (**III**) $k_\alpha = 66.19\%$ and $k_\beta = 16.62\%$. These slip angles percentages were reported by Scheding et al. (1999) from experimental trails developed in underground mining using an RS vehicle

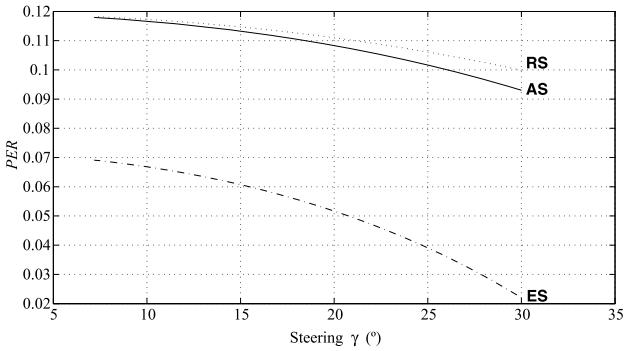

Fig. 11 Positioning error ratio for Ackermann, Articulated and Explicit steering while turning a specific steering angle γ at $k_\alpha = 66.19\%$ and $k_\beta = 16.62\%$

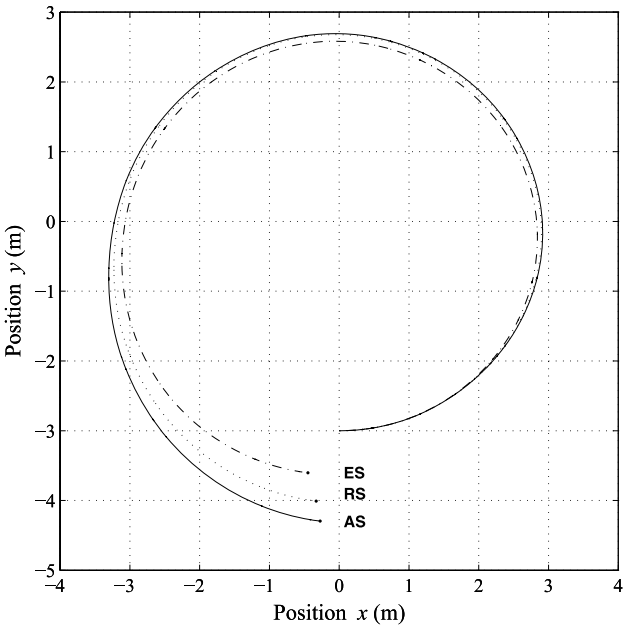

Fig. 12 Accumulated PER of Ackermann, Articulated and Explicit vehicles while performing a steady turn ($R = 3$ m), under identical magnitude of slip angle percentages and independent on steering angle

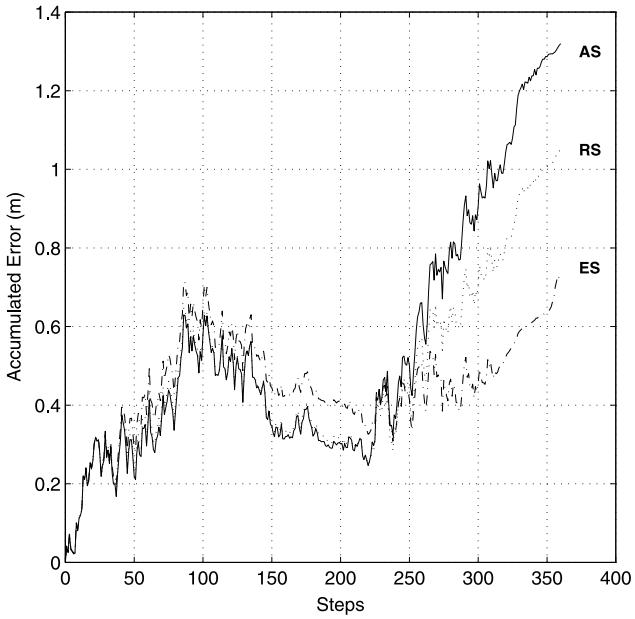

Fig. 13 Accumulated error of Ackermann, Articulated and Explicit vehicles while performing a steady turn. The error is calculated as the distance between the ideal position and the position that the vehicle experienced due to slip angles

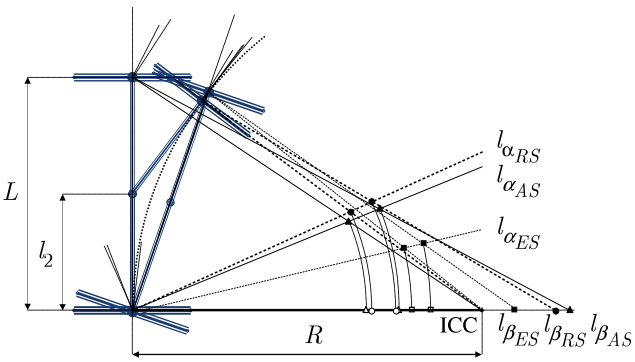

Fig. 14 Geometric positioning error comparison for AS, RS and ES vehicles. The slip effect is represented by perpendicular lines to the slip angles ($l_{\alpha_{AS}}$, $l_{\alpha_{RS}}$, $l_{\alpha_{ES}}$, $l_{\beta_{AS}}$, $l_{\beta_{RS}}$ and $l_{\beta_{ES}}$). The intersection of these lines for AS (△), RS (○), and ES(◇) represents a new instantaneous center of curvature and its projection on the ideal radius shows the difference

perform a complete turn. This is shown in Figs. 12 and 13, where we assume the RS slip angles from Fig. 8 are applied to the three vehicles. This advantage is correlated to the relationship L/R and the number of degrees of freedom required to steer the vehicle, which is captured in the kinematic model. The ES vehicle, actuating as a double Ackermann steering, is considered with a rear steering angle and a front steering angle (two degrees of freedom). Both AS and RS vehicles have only one degree of freedom to steer the vehicle.

These observations may be interpreted geometrically through Fig. 14, which shows the effect on radius induced by slip angles for three vehicles while performing an ideal radius R turn. The wheelbases L and the steering angles are identical. The slip effect is represented by perpendicular lines to the slip angles, which are denoted as $l_{\alpha_{AS}}, l_{\alpha_{RS}}, l_{\alpha_{ES}}$, $l_{\beta_{AS}}, l_{\beta_{RS}}$, and $l_{\beta_{ES}}$. The respective intersection represents a new instantaneous center of curvature (ICC). Its projection on the ideal radius allows us to observe the change of radius that the vehicle experiences due to the slip angles.

Based on the results, the effects of the slip angles were related as a centrifugal behavior, due to the positive values of the slip angles. Taking the signs of the slip angles as centrifugal and spinning effects, the PER equations leads to a fuller observation. It is evident that the term $1/\sin(\gamma + \alpha - \beta)$ or $1/\sin(2\gamma + \alpha - \beta)$, leads to the effects of the slip angles for AS, RS, and ES vehicles, respectively.

Clearly, this term is not defined at $\sin(\gamma + \alpha - \beta) = 0$. For negative values of α and positive values of β, as $|\beta| + |\alpha|$ becomes closer and closer to γ for AS and RS vehicles and 2γ for ES vehicle, respectively. The value of the term begins to grow rapidly and approaches the worst case.

7 Conclusions

The contribution of this paper is the introduction of a positioning error analysis for wheeled robotic vehicles. It is an aid to in-depth evaluation and comparison of steering geometries under equal operation conditions, while increasing the understanding of their fundamental differences. Analytical expressions derived from reformulated kinematic models are used to relate the performance of the robotic vehicle to the factors that affect this error.

The analytical comparison between alternative candidates and critical actions of the robotic vehicle (i.e. position estimation) addresses the selection of the steering mechanism, and gives the direction to enhance the control and safeguarding capabilities. It is important to note that beyond the impact in the selection process, the numerical results of the performance for every candidate vehicle allow a quantitative interpretation of their advantages and drawbacks to perform the pursued task in the expected conditions of operation.

Acknowledgements This work has been supported by Consejo Nacional de Ciencia y Tecnología (CONACyT) under grants 35396 and 144471. The authors would also like to thank the Robotics Institute of the Carnegie Mellon University, Tecnológico de Monterrey and the Centro de Investigaciones Biológicas del Noroeste. Their support is gratefully acknowledged.

References

Alexander, J. C., & Maddocks, J. H. (1989). On the kinematics of wheeled mobile robots. *International Journal of Robotics Research*, *8*(5), 15–27.

Altafini, C. (1999a). A path-tracking criterion for an lhd articulated vehicle. *The International Journal of Robotics Research*, *18*(5), 435–441.

Altafini, C. (1999b). Why to use an articulated vehicle in underground mining operations? In *Prococeedings of the IEEE international conference on robotics and automation* (Vol. 4, pp. 3020–3025), May 1999.

Apostolopoulos, D. (2001). *Analytical configuration of wheeled robotic locomotion*. PhD thesis, The Robotics Institute, Carnegie Mellon University.

Barshan, B., & Durrant-Whyte, H. F. (1995). Inertial navigation system for mobile robots. *IEEE Transactions on Robotics and Automation*, *11*(3), 328–342.

Borenstein, J., Everett, H. R., Feng, L., & Wehe, D. (1997). Mobile robot positioning and sensors and techniques. *Journal of Robotic Systems, Special Issue on Mobile Robots*, *14*(4), 231–249.

Campion, G., Bastin, G., & D'Andra-Novel, B. (1996). Structural properties and classification of kinematic and dynamic models of wheeled mobile robots. *IEEE Transactions on Robotics and Automation*, *12*(1), 47–62.

Cannon, H. N. (1999). *Extended earthmoving with an autonomous excavator*. Master's thesis, The Robotics Institute Carnegie Mellon University.

Chung, H., Ojeda, L., & Borenstein, J. (2001). Accurate mobile robot dead-reckoning with a precision-calibrated fiber optic gyroscope. *IEEE Transactions on Robotics and Automation*, *17*(1), 80–84.

Colyer, R. E., & Economou, J. T. (1998). Comparison of steering geometries for multi-wheeled vehicles by modelling and simulation. In *Proceedings of the 37th IEEE conference on decision and control* (Vol. 3, pp. 3133–3133), December 1998.

Coombs, D., Murphy, K., Lacaze, A., & Legowik, S. (2000). Driving autonomously offroad up to 35 km/h. In *Proceedings of the 2000 intelligent vehicles conference*, October 2000.

Dissanayake, M. W. M. G., Newman, P., Clark, S., Durrant-Whyte, H. F., & Csorba, M. (2001). A solution to the simultaneous localization and map building (slam) problem. *IEEE Transactions on Robotics and Automation*, *17*(3), 229–241.

Dixon, J. C. (1996). *Tires, suspension, and handling*. Society of Automotive Engineers.

Dudzinski, P. A. (1989). Design characteristics of steering systems for mobile wheeled earthmoving equipment. *Journal of Terramechanics*, *26*(1), 25–82.

Everett, H. R. (1995). *Sensors for mobile robots: theory and application*. Wellesley: Peters.

Fiorini, P. (2000). Ground mobility systems for planetary exploration. In *IEEE international conference on robotics and automation* (Vol. 1, pp. 908–913), 24–28 April 2000.

Fong, T. W., Thorpe, C., & Glass, B. (2003). Pdadriver: A handheld system for remote driving. In *IEEE international conference on advanced robotics*, July 2003.

Gambao, E., & Balaguer, C. (2002). Robotics and automation in construction. *IEEE Robotics and Automation Magazine*, *9*(1), 4–6.

Gillespie, T. D. (1992). *Fundamentals of vehicle dynamics*. Society of Automotive Engineers.

Gutierrez, J., Gordillo, J. L., & Lopez, I. (2004). Configuration and construction of an autonomous vehicle for a mining task. In *IEEE international conference on robotics and automation* (Vol. 3, pp. 2010–2016), 25 April–5 May 2004.

Kelly, A. (2004). Linearized error propagation in odometry. *International Journal of Robotics Research*, *23*(2), 179–213.

Large, F., Sekhavat, S., Laugier, C., & Gauthier, E. (2000). Towards robust sensor-based maneuvers for a car-like vehicle. In *Proceedings IEEE international conference on robotics and automation* (Vol. 4, pp. 3765–3770).

Latombe, J. C. (1991). *Robot motion planning*. Boston: Kluwer Academic.

Laumond, J. P. (1993). Controllability of a multibody mobile robot. *IEEE Transactions on Robotics and Automation*, *9*(6), 755–763.

Muir, P. F., & Neuman, C. P. (1987). Kinematic modeling of wheeled mobile robots. *Journal of Robotic Systems*, *4*(2), 281–340.

Muirhead, B. K. (2004). Mars rovers, past and future. In *Proceedings of 2004 IEEE aerospace conference* (Vol. 1, pp. 128–134), March 2004.

Pilarski, T., Happold, M., Pangels, H., Ollis, M., Fitzpatrick, K., & Stentz, A. (2002). The demeter system for automated harvesting. *Autonomous Robots*, *13*, 9–20.

Redmill, K., & Ozguner, U. (1999). The Ohio state university automated highway system demonstration vehicle. *SAE Transactions 1997: Journal of Passenger Cars, Society of Automotive Engineerings*.

Rollins, E., Luntz, J., Foessel, A., Shamah, B., & Whittaker, W. (1998). Nomad: A demonstration of the transforming chassis. In *IEEE international conference on robotics and automation* (Vol. 1, pp. 611–617), 16–20 May 1998.

Samson, C. (1995). Control of chained systems application to path following and time-varying point-stabilization of mobile robots. *IEEE Transactions on Automatic Control*, *40*(1), 64–77.

Scheding, S., Dissanayake, G., Nebot, E., & Durrant-Whyte, H. (1997). Slip modelling and aided inertial navigation of an lhd. In *Proceedings IEEE international conference on robotics and automation* (pp. 1904–1909), April 1997.

Scheding, S., Nebot, E., Stevens, S., Durrant-Whyte, H., Roberts, J., Corke, P., Cunningham, J., & Cook, B. (1999). An experiment in autonomous navigation of an underground mining vehicle. *IEEE Transactions on Robotics and Automation*, *15*(1), 85–95.

Shiller, Z., & Sundar, S. (1998). Emergency lane-change maneuvers of autonomous vehicles. *ASME Journal of Dynamic Systems, Measurement, and Control*, *120*(1), 37–44.

Stentz, A. (2001). Robotic technologies for outdoor industrial vehicles. In *SPIE aerosense*.

Stentz, A., Bares, J., Singh, S., & Rowe, P. (1999). A robotic excavator for autonomous truck loading. *Autonomous Robots*, *7*(2), 175–186.

Stombaugh, T. S. (1998). *Automatic Guidance of Agricultural Vehicles at Higher Speeds*. PhD thesis, Agriculture Engineering, University of Illinois at Urbana-Champaign.

Thorpe, C. (1997). Mobile robots and smart cars. In *First international conference on field and service robotics*, December 1997.

Thrun, S., Haehnel, D., Ferguson, D., Montemerlo, M., Triebel, R., Burgard, W., Baker, C., Omohundro, Z., Thayer, S., & Whittaker, W.L. (2003). A system for volumetric robotic mapping of abandoned mines. In *IEEE international conference on robotics and automation* (Vol. 3, pp. 4270–4275), 14–19 September 2003.

Trebi-Ollennu, A., & Dolan, J. M. (1999). *An autonomous ground vehicle for distributed surveillance: cyberscout*. Technical Report ICES-04-09-99.

Tunstel, E., Huntsberger, T., Trebi-Ollennu, A., Aghazarian, H., Garret, M., Leger, C., Kennedy, B., Baumgartner, E., & Schenker, P. (2002). Fido rover system enhancements for high-fidelity mission simulation. In *Proceedings of the 7th international conference on intelligent autonomous systems* (pp. 349–356), March 2002.

Joaquín Gutiérrez is a researcher at the Centro de Investigaciones Biológicas del Noroeste, S.C. (CIBNOR). His current research interests include the development and experimental validation of robotic systems for biological research applications. He received his B.S. degree in Communications and Electronics Engineering in 1988 from the Instituto Politécnico Nacional, México and Ph.D. degree in Artificial Intelligence in 2004 from the Instituto Tecnológico y de Estudios Superiores de Monterrey, México. He joined at CIBNOR in 1988 and led several engineering projects in embedded microcontroller systems. He enrolled at the Tecnológico de Monterrey and joined at the group of Autonomous Vehicles at the Center for Intelligent Systems from 1999 to 2004.

Dimitrios Apostolopoulos is a Senior Systems Scientist at the Robotics Institute of Carnegie Mellon University, Pittsburgh, PA. His work focuses on robotics for discovery and exploration, and as a workforce in extreme applications and for hazardous duty on Earth and beyond. In the last 10 years Dr. Apostolopoulos has led high-profile robotics programs for space, defense, and private industry applications. Significant accomplishments of his work include the creation, development, and successful validation of robots for autonomous search of Antarctic meteorites, robots for long-range missions in polar environments, robust unmanned ground vehicles for USMC combat missions, hopping robots for all-terrain mobility, and reconfigurable and inflatable robotic locomotion systems for Mars exploration. His areas of expertise include robot design, robotic mobility, mechatronics, mechanisms, analysis, and control. Dr. Apostolopoulos holds a Ph.D. in Robotics from Carnegie Mellon.

José Luis Gordillo graduated in industrial engineering from the Technological Institute of Aguascalientes, Mexico. He obtained both the D.E.A. degree and the Ph.D. in Computer Science from the National Polytechnic Institute of Grenoble, France, in 1983 and 1988, respectively. From 1989 to 1990 he was Assistant Professor at the Department of Automatic Control of the Center for Advanced Studies and Research of the National Polytechnic Institute of Mexico (CINVETAV-IPN). Currently he is Full Professor at the Center for Intelligent Systems at the Tecnológico de Monterrey (ITESM). He has been a Visitor Professor in the Computer Science Robotics Laboratory at Stanford University (1993), at the Project Sharp of INRIA Rhone-Alpes in France (2002 and 2004) and some other universities and research institutes. His research interests are in computer vision for robotics applications, in particular autonomous vehicles, and the development of virtual laboratories for education and manufacturing. He participated and leaded R&D projects with industry like Honewell Bull in France, Sun Microsystems, Peñoles and TV Azteca; and government entities like the Center for the Atomic Energy (CEA) in France, the Mexican Army, the French-Mexican Laboratory for Computer Science (LaFMI), the Institute of the Water of the Nuevo Leon state (IANL), and the National Council for Science and Technology in Mexico (CONACyT).